DDSRF Theory based Solar assisted RELIFT Luo Converter with UPQC used in Voltage Enhancement

M.VENKATESWARLU[1,*], B PAKKIRAIAH[2], B LOVESWARA RAO[1]
[1]Department of Electrical and Electronics Engineering,
Koneru Lakshmaiah Education Foundation,
Vaddeswaram, Guntur, Andhra Pradesh-522502,
INDIA

[2]Department of Electrical and Electronics Engineering,
Gokaraju Rangaraju Institute of Engineering and Technology-Autonomous,
Hyderabad-500090,
INDIA

**Corresponding Author*

Abstract: - As PV system-based power generation and sensitive non-linear loads are integrated more frequently, there is a greater need for enhanced Power Quality (PQ) in distributed power systems. In this work, a specialized power device known as a Unified Power Quality Conditioner (UPQC) is proposed to improve the PQ of the network overall. Source and load side PQ related issues are addressed using series and shunt compensators in order. The PV system can provide active power to the load in the presence of the shunt compensator. Using the Re-lift Luo DC-DC converter, the output voltage of the PV system is increased which further improves the voltage gain and efficiency of the intended converter. An FLC is utilized to adjust the gain values of the pi Controller which further improves the voltage profile of the UPQC. Decoupled Double Synchronous Reference Frame (DDSRF) theory is utilized to produce the reference current and voltage values to improve the current-voltage profiles at the source end. To attain the controlled responses of the shunt and series compensators Type-2 FLC (CT2FLC) based controllers are utilized.

Key-Words: - DDSRF Theory, PV-UPQC, Adaptive PI controller, CT2FLC, Re-lift Luo converter, FL Controller, DSTATCOM.

Received: April 19, 2024. Revised: October 2, 2024. Accepted: November 3, 2024. Published: December 2, 2024.

1 Introduction

To attain the suitable PQ of the system, different types of loads are connected sequentially. The operation of sensitive devices that are connected to the power systems depends on the PQ of the system supplied by the generating station, especially at low values of the PQ. To avoid the failure of the devices in the systems, power should be supplied within the limits only, [1], [2]. Power quality (PQ) problems, which show as distribution system voltage variations, are mostly caused by the power electronic loads' non-linear current drawing behavior, [3]. Additionally, the emphasis on generating clean energy has led to a rise in the usage of PV in distributed power networks, which increases the risk of voltage instability due to its intermittent nature. In addition to capacitor bank heating, these voltage instability problems cause frequent false triggering, false tripping, and failure of the electrical devices, [4], [5]. A three-phase solar energy conversion system with many functions that can adjust for load-side PQ problems is proposed in [6]. In addition to renewable energy generation, a shunt active filtering based on the Distribution Static Compensator (DSTATCOM) is proposed in [7], [8]. Reactive power injection is a trade-off for DSTATCOM's superior load voltage management. As a result, DSTATCOM cannot keep grid current unity power factor and PCC voltage regulation simultaneously. A series of active filtering devices called a Dynamic Voltage Resonator (DVR), [9], has been suggested recently to meet the high PQ requirements of subtle loads.

To gain the extra benefit of producing decarbonized electricity, PV-based DVR setups are designed in [10], [11]. A UPQC, [12], [13], with both shunt active filtering and series active filtering is preferable over DVR and DSTATCOM. By

employing an appropriate controller strategy in conjunction with the converter, the PV system's intermittency-related limitation can be removed. By controlling its duty cycle, stabilizes the high-voltage output. The PV system's voltage level is improved by choosing a Re-lift Luo converter. The PI controller is a popular linear controller method for managing a power electronic converter's operation. Nevertheless, because it is a fixed gain controller, it cannot adjust to changes in the system's parameters or the environment.

Consequently, an FLC is utilized to adjust the PI controller's gain values, improving its dynamic response and enabling a wider range of operating circumstances for which it may be used, [14], [15], [16]. To regulate the UPQC, the cascaded control technique, [17], including two T2FLCs is suggested. Using DDSRF Theory, the primary objective of reference signal creation is completed. A radial basic neural network forms the basis of the created genetic algorithm model. These neural networks make it feasible to solve technological and financial issues that call for high-speed processing while also minimizing the expense of data processing time. The suggested method enables the most precise and rational choice to be made when utilizing renewable energy sources to address the issue of active power reserves, [18]. A method for autonomous monitoring and management is presented that enables the identification and tracking of degradation on structural elements and joints of steel constructions that are currently in place, [19], [20]. The article uses a Field-Programmable Gate Array (FPGA) board and related computer-aided design (CAD) tool to propose, develop, model, and verify the reconfigurable gates and core components of the CPU. Through the use of testing programs, the implemented processor demonstrated its flexibility in reconfiguration, [21]. Junction gate field-effect transistor (JFET) is utilized for low forward voltage drop application point of view which is combination of the silicon carbide, is the basis of the unique hybrid diode concept known as the Huang-Pair, [22]. This article investigates approaches for employing distinct low-voltage diodes in series as one high-voltage diode in high-frequency applications. As a result of the parasitic capacitance from the physical diode linkages to common, we find that series-linking diodes can lead to higher loss as well as imbalances in temperature and voltage among the diodes, [23]. This work presents a PV-UPQC that supports both carbon-negative power generation and increased PQ. Re-lift Luo converter and fuzzy-tuned adaptive PI controller are used to provide a PV system with a stable, regulated, and elevated voltage level. Control over the operation of the UPQC's series and shunt compensators is established utilizing a CT2FLC in addition to DDSRF theory.

2 Proposed System Description

A utility system's primary duty is to supply customers with electricity in the form of pure sinusoidal at PCC that is appropriate in frequency and magnitude. To increase the PQ of the distributed power system, a PV-UPQC is therefore given the further advantage of carbon-free power generation shown in Figure 1.

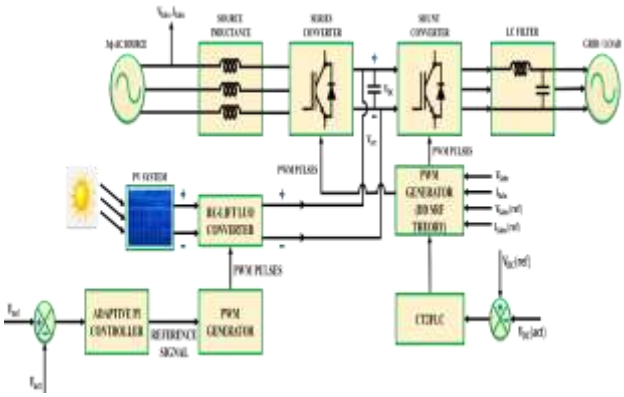

Fig. 1: Complete block diagram representation of the PV-UPQC

The Adaptive PI controller receives the error value that results from comparing the Re-lift Luo converter's actual voltage with the set reference voltage. The PWM generator creates pulses to operate the switches of the Re-lift Luo converter with the help of the reference control signal produced by the controller. Regarding UPQC, the shunt converter decreases issues with current harmonics on the load side and the series converter decreases issues with voltage quality on the source side. The reference and actual DC-link voltages $(V_{DC}(ref), V_{DC}(act))$, are compared, and the voltage error is determined before being forwarded to the CT2FLC for processing. The reference voltage signal for stabilizing source voltage changes and the reference current signal for reducing load side current harmonics are produced using DDSRF theory. Finally, the PV-UPQC configuration that has been recommended improves the PQ of the source side and load side.

3 Proposed System Modelling

The proposed research [19], proposes a method that uses just manufacturer-provided data to track the

maximum power point of a solar panel or photovoltaic field under various climatic circumstances. The method is based on the mathematical model of a diode.

3.1 PV Fed Re-Lift Luo Converter

As can be seen in Figure 2, the single diode model serves as the foundation for the construction of the PV module, which contains many PV cells. Additionally, the PV cell's output current is provided as:

$$I_{pv} = I_{ph} - I_0\left[exp\left(\frac{q(V+IR_S)}{N_S KTA}\right) - 1\right] - (V + IR_s)/(R_p) \quad (1)$$

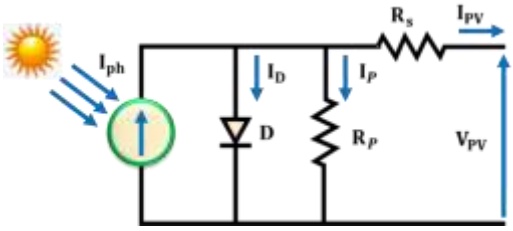

Fig. 2: Electrical model representation of the PV cell

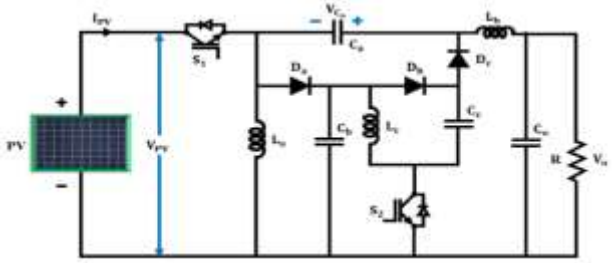

Fig 3: Re-lift Luo converter general representation

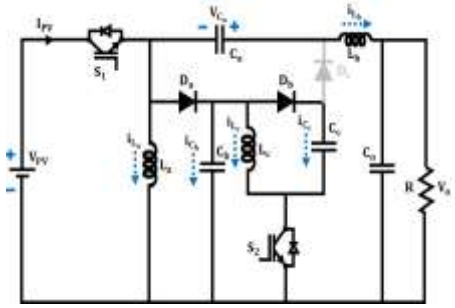

(a)

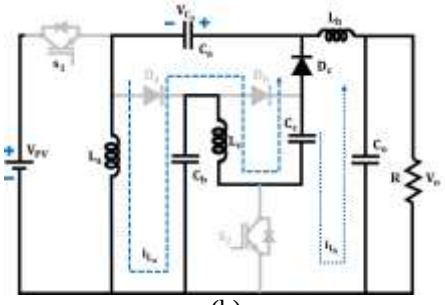

(b)

Fig. 4: Different operation modes of the Re-lift Luo converter

3.1.1 Mode 1

In this mode, the inductors L_a and L_c is absorbed from the source energy when both switches are in the ON position. Both the input source and the capacitor C_a provide the inductor's energy, or L_b. In this mode, there is a linear increase in currents i_{L_a}, i_{L_b} *and* i_{L_c}.

3.1.2 Mode 2

As opposed to mode 1, where the source current I_{PV} is equal to zero and both switches are in the OFF state. When the current i_{L_a} and i_{L_b} charges the capacitor C_a, the capacitor receives the energy that the inductor has stored. Throughout this mode, the currents i_{L_a} and i_{L_b} both decreases.

The peak-to-peak fluctuation of current i_{L_c} during mode 1 is provided as follows:

$$\Delta i_{L_c} = \frac{V_{PV} kT}{L_c} \quad (2)$$

The fluctuation is comparable to the mode 2 current decrease,

$$\Delta i_{L_c} = \frac{V_{L_c}(1-k)T}{L_c} \quad (3)$$

When mode 2 is in effect, the voltage drops across the inductor L_c is as follows:

$$V_{L_c} = \frac{k}{1-k} V_{PV} \quad (4)$$

In mode 1, the current i_{L_a} grows throughout the time interval kt, while in mode 2, it decreases during the interval (1-k) t.

$$kTV_{PV} = (1-k)T(V_{C_a} - 2V_{PV} - V_{L_c}) \quad (5)$$

The following represents the voltage V_{C_a} across the capacitor:

$$V_{C_a} = \frac{2}{1-k} V_{PV} \quad (6)$$

In addition, the current i_{L_b} simultaneously rises in mode 1 and falls in mode 2. Therefore,

$$kT\left(V_{C_a} + V_{PV} - V_o\right) = (1-k)T(V_o - 2V_{PV} - V_{L_c}) \quad (7)$$

Given is the output voltage, or V_o.

$$V_o = \frac{2}{1-k} V_{PV} \quad (8)$$

This is the output current given:

$$I_o = \frac{1-k}{2} I_{PV} \quad (9)$$

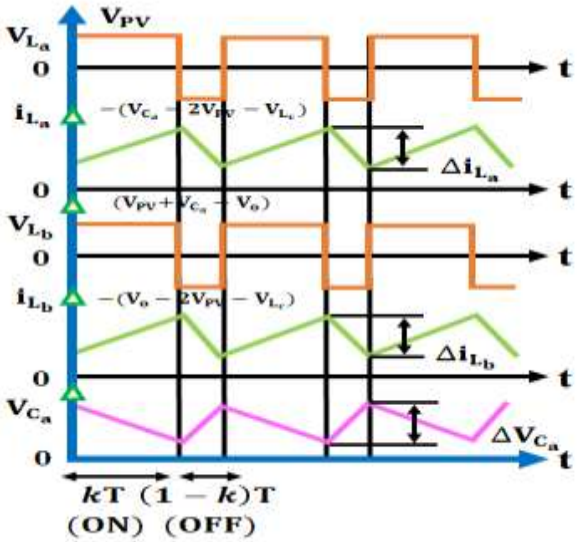

Fig. 5: Operation related wave forms of the Re-Lift Luo converter

The inductor L_a has the following value:

$$L_a = \frac{kTV_{PV}}{\Delta i_{L_a}} \tag{10}$$

The inductor L_b has a value of

$$L_b = \frac{kTV_{PV}}{\Delta i_{L_b}} \tag{11}$$

The capacitors C_a, C_b, C_c and C_o can be valued using the following formulas:

$$C_a = \frac{(1-k)Ti_{L_a}}{\Delta V_{C_a}} = \frac{(1-k)kT}{\Delta V_{C_a}} I_{PV} \tag{12}$$

$$C_b = \frac{(1-k)T(i_{L_a}+i_{L_b})}{\Delta V_{C_b}} = \frac{I_o T}{\Delta V_{C_b}} \tag{13}$$

$$C_c = \frac{(1-k)T(i_{L_a}+i_{L_b})}{\Delta V_{C_c}} = \frac{I_o T}{\Delta V_{C_c}} \tag{14}$$

$$C_o = \frac{kT^2 V_{PV}}{4\Delta V_o L_b} \tag{15}$$

A fuzzy tuned PI controller is used in this study to improve the Re-lift Luo converter's transient response.

3.2 Fuzzy Tuned Adaptive PI Controller

The extensive use of conventional PI controllers in various industrial applications can be attributed to their advantageous features, including their quick reaction time and ease of setup. However, because it is a fixed gain controller, it is less able to adjust to changes in the system parameters and the environment. Thus, in this work, an Adaptable PI controller is used, which combines the quick response of a PI controller with the independent and adaptive properties of an FLC. Unlike the traditional PI controller, the gains K_P *and* K_I are estimated using the FLC and are tunable as opposed to fixed. Figure 6 depicts the Re-lift Luo converter architecture with an Adaptive PI controller.

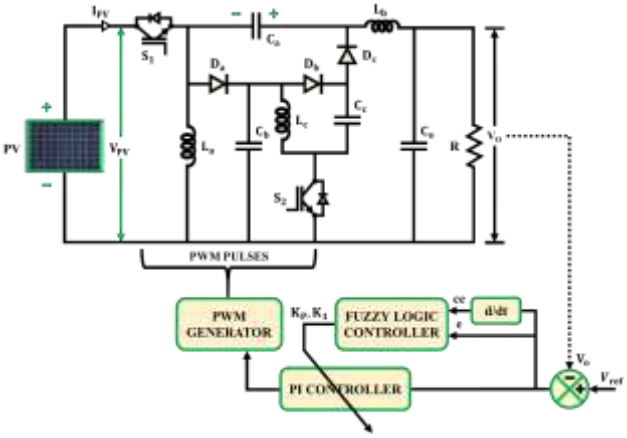

Fig. 6: PI controller with adaptability for Re-lift Luo converter

Due to the adaptive PI controller's selection for controlling the Re-lift Luo converter's output voltage, the voltage error (e) and change in voltage error (ce) serve as the FLC's input variables. As shown in Figure 7(a), five triangle membership functions are assigned to each of these two input variables. The linguistic variables Positive Large (PL), Positive Small (NS), Zero (Z), Negative Large (NL), and Positive Small (NS) in Figure 7 are used to express the fuzzy variables for the inputs. The Min-Max approach and the center of gravity are utilized for the purposes of fuzzy inference and defuzzification, respectively. As can be seen in Table 1, the FLC uses two rule bases to estimate the values of the PI gains, or K_P *and* K_I.

Table 1. PI Gain rules based on the basic rules

Output (K_P)		Error (e)				
		NL	NS	Z	PS	PL
Change in Error (ce)	NL	L	L	M	M	S
	NS	L	L	M	S	S
	Z	M	M	M	M	M
	PS	S	M	M	M	L
	PL	S	S	M	L	L
Output (K_I)		**Error (e)**				
		NL	NS	Z	PS	PL
Change in Error (ce)	NL	S	S	M	L	L
	NS	S	S	M	L	L
	Z	M	M	M	M	M
	PS	L	L	M	S	S
	PL	L	L	M	S	S

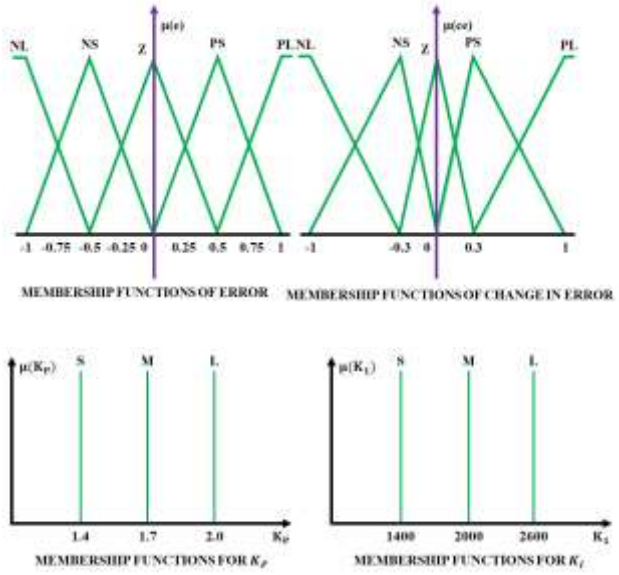

Fig. 7: Membership functions for the variables' (a) input and (b) output

The rules are created using information on how the converter works, different types of errors, and changes in error inputs. The firing strength for each rule i is provided as follows:

$$\mu_i = \prod_{j=1}^{2} A_{ij} \tag{16}$$

where the membership function is denoted by A_{ij}.

The labels $c_i \; and \; v_i$ are used to represent the singleton values. The FLC's outputs are provided as follows:

$$K_P = \frac{\sum_{i=1}^{r} c_i \mu_i}{\sum_{i=1}^{r} \mu_i} \tag{17}$$

$$K_I = \frac{\sum_{i=1}^{r} v_i \mu_i}{\sum_{i=1}^{r} \mu_i} \tag{18}$$

where r is the number of rules. As a result, the output signal that the PI controller produced is as follows:

$$u = K_P e + K_I \int e \, dt \tag{19}$$

3.3 Modelling of UPQC

The UPQC makes sure that the loads connected to the distributed power system always receive power that meets the necessary standards and specifications. Shunt compensators are used to reduce load side PQ problems like reactive power and harmonics, whereas series compensators are used to reduce grid side PQ problems like sag/swell. Furthermore, by injecting current into the load side, the former improves PQ, and by injecting voltage into the grid side, the latter improves PQ. These factors were taken into account when creating the UPQC

3.3.1 DC-link Voltage Magnitude

The lowest DC-link voltage value is calculated based on the phase voltage of the system and is stated as,

$$V_{dc,min} = \frac{2\sqrt{2}(V_{LL,rms})}{\sqrt{3}(m)} \tag{20}$$

where m is the modulation depth and $V_{LL,rms}$ represents the phase-voltage of the grid.

3.3.2 Shunt Compensator DC-link Capacitor Value

The following formula is used to express the DC-link capacitor's capacitance value:

$$C_{dc,min} = \frac{3V_{ph} i_{sh} a_f k_e t}{1/2({V_{dc,ref}}^2 - {V_{dc,min}}^2)} \tag{21}$$

where the words$i_{sh} \; and \; V_{ph}$, respectively, are used to specify the phase-current and phase-voltage of the shunt compensator. The overloading factor is denoted as a_f, the reference voltage is denoted as $V_{dc,ref}$, and the energy variation under dynamic conditions is designated as k_e.

3.3.3 Inductor Ripple Filter

The following formula is used to express the value

$$L_{f,min} = \frac{(\sqrt{3})(m)(V_{dc,ref})}{12(a_f)(f_S)(I_{cr})} \tag{22}$$

In this case, the switching frequency is denoted as f_S and the inductor ripple current is provided as I_{cr}.

3.3.4 Series Injection Transformer

The turns ratio in the case of a series transformer is provided as follows:

$$K_{SE} = \frac{V_{LLrms}}{\sqrt{3}(V_{SE})} \tag{23}$$

The VA rating of the transformer is listed as:

$$S_{SE} = 3(V_{SE})(i_{SE_{(under\ sag)}}) \tag{24}$$

The current flowing through a series compensator is equal to the grid current.

3.3.5 Series Compensator Inductor Ripple Filter

The specified inductor ripple filter is

$$L_{r,min} = \frac{(\sqrt{3})(m)(V_{dc,ref})(K_{SE})}{12(a_f)(f_S)(I_r)} \tag{25}$$

In this case, the inductor ripple current is denoted by I_r . With the use of CT2FLC and DDSRF theory, control over the series and shunt compensators is enabled.

3.4 Modelling of CT2FLC

CT2FLC, which consists of two Type 2-FLC, is in responsible for regulating the operation of UPQC (T2FLC). The T2-FLC is utilised in this work instead of its counterpart, the T1-FLC, since it is more equipped to handle problems involving non-linearity and uncertainty. The second T2FLC receives its input as the control signal from the first T2FLC.

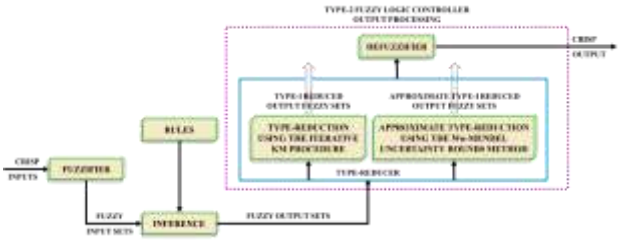

Fig. 8: The complete architecture of the T2FLC

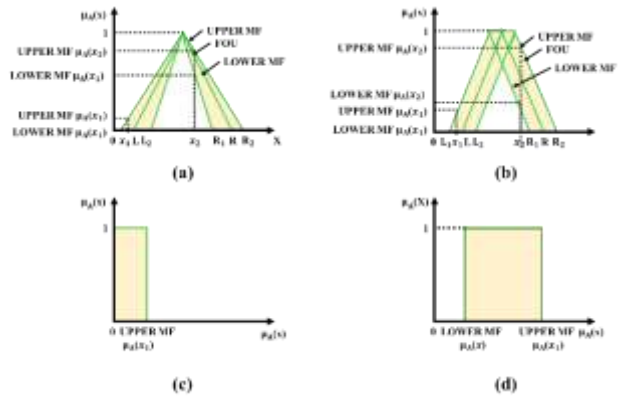

Fig. 9: The FOU representation related to T2FLC

The configuration of T2FLC, which is a logical extension of T1FLC and provides more details in the secondary membership function, is shown in Figure 8. The former differs from the later in that it lacks the defuzzifier section and instead has an output processing block. The output processing module contains a type reducer and the defuzzification block. Figure 9 illustrates how it makes use of the footprint of uncertainty (FOU) idea. The fuzzification block's job is to convert the input numeric vector $X = (x_1, x_2, \dots, x_p)^T \in X_1 \times X_2 \times \dots \times X_p \equiv X$. The input mapping is provided as:

$$\mu_{\widetilde{A_x}}(x) = 1/1 \ and \ x = x' \quad (26)$$

$$\mu_{\widetilde{A_x}}(x) = 1/0 \ for \ \forall x \in x \ \ with \ \ x \neq x' \quad (27)$$

The T2FLC rule structure is written as:

$$R^i: IF x_1 is \widetilde{F_1^i} and \dots and \ x_p \ is \ \widetilde{F_p^i}, THEN \ Y^i = C_0^i + C_1^i x_1 + \dots + C_p^i x_p \quad (28)$$

The fuzzy sets T1 consequent and T2 antecedent are represented by $C_j^i (j = 0,1, \dots, p)$ and $\widetilde{F_k^i} (k = 1, \dots, p)$, respectively. Y^i is the output's specified value. The inference engine uses the fuzzy sets to create mappings. Union and intersection operations are computed to realise these mappings. The output of the defuzzifier is evaluated using the type reduced set (y_1, y_r) that is produced from the type reducer. This output is presented as:

$$y(x) = \frac{y_1 + y_r}{2} \quad (29)$$

Consequently, the UPQC's operation is managed by the CT2FLC.

3.4.1 DDSRF Theory

The following formula can be used to express the negative, positive, and zero components of a three-phase power system:

$$\begin{bmatrix} V_{as} \\ V_{bs} \\ V_{cs} \end{bmatrix} = V_0 \begin{bmatrix} y(\omega t + \phi_0) \\ y(\omega t + \phi_0) \\ y(\omega t + \phi_0) \end{bmatrix} + V_1 \begin{bmatrix} y(\omega t + \phi_1) \\ y(\omega t - \frac{2\pi}{3} + \phi_1) \\ y(\omega t + \frac{2\pi}{3} + \phi_1) \end{bmatrix} + V_2 \begin{bmatrix} y(\omega t + \phi_2) \\ y(\omega t - \frac{2\pi}{3} + \phi_2) \\ y(\omega t + \frac{2\pi}{3} + \phi_2) \end{bmatrix} \quad (30)$$

The symbol for the asymmetrical source voltage is:

$$V_s = \begin{bmatrix} V_{as} \\ V_{bs} \\ V_{cs} \end{bmatrix} = \begin{bmatrix} V_{a0} \\ V_{b0} \\ V_{c0} \end{bmatrix} + \begin{bmatrix} V_{a1} \\ V_{b1} \\ V_{c1} \end{bmatrix} + \begin{bmatrix} V_{a2} \\ V_{b2} \\ V_{c2} \end{bmatrix} \quad (31)$$

Given is the source current component:

$$I_s = \begin{bmatrix} I_{as} \\ I_{bs} \\ I_{cs} \end{bmatrix} = \begin{bmatrix} I_{a0} \\ I_{b0} \\ I_{c0} \end{bmatrix} + \begin{bmatrix} I_{a1} \\ I_{b1} \\ I_{c1} \end{bmatrix} + \begin{bmatrix} I_{a2} \\ I_{b2} \\ I_{c2} \end{bmatrix} \quad (32)$$

The three-phase voltage is changed as follows using Clark's transformation:

$$V_{\alpha\beta 0} = \frac{2}{3} \begin{bmatrix} 1 & -\frac{1}{2} & -\frac{1}{2} \\ 0 & \frac{\sqrt{3}}{2} & -\frac{\sqrt{3}}{2} \\ \frac{1}{2} & \frac{1}{2} & \frac{1}{2} \end{bmatrix} V_s \quad (33)$$

$$I_{\alpha\beta 0} = \frac{2}{3} \begin{bmatrix} 1 & -\frac{1}{2} & -\frac{1}{2} \\ 0 & \frac{\sqrt{3}}{2} & -\frac{\sqrt{3}}{2} \\ \frac{1}{2} & \frac{1}{2} & \frac{1}{2} \end{bmatrix} I_s \quad (34)$$

The three-phase current is changed as follows using Clark's transformation:

Following the removal of the zero-sequence element:

$$V_{\alpha\beta}=\frac{2}{3}\begin{bmatrix}1 & -\frac{1}{2} & -\frac{1}{2}\\ 0 & \frac{\sqrt{3}}{2} & -\frac{\sqrt{3}}{2}\end{bmatrix}V_s \quad (35)$$

$$I_{\alpha\beta0}=\frac{2}{3}\begin{bmatrix}1 & -\frac{1}{2} & -\\ 0 & \frac{\sqrt{3}}{2} & -\frac{\sqrt{3}}{2}\end{bmatrix}I_s \quad (36)$$

The power, both actual and imagined, is granted as:

$$\begin{bmatrix}p\\ q\end{bmatrix}=\begin{bmatrix}V_\alpha & V_\beta\\ -V_\beta & V_\alpha\end{bmatrix} \quad (37)$$

The resultant voltage is given as:

$$V_{\alpha\beta}=V_1\begin{bmatrix}\cos(\omega t+\phi_1)\\ \sin(\omega t+\phi_1)\end{bmatrix}+V_2\begin{bmatrix}\cos(-\omega t+\phi_2)\\ \sin(-\omega t+\phi_2)\end{bmatrix} \quad (38)$$

The angular frequency of the rotating coordinate system and the voltage vector have the same frequency in a stationary reference frame. The state of DDSRF is determined by applying a Park's transformation to separate the positive and negative sequence components.

$$V_{dq1}=V_{\alpha\beta}\begin{bmatrix}\cos(\omega t) & -\sin(\omega t)\\ -\sin(\omega t) & \cos(\omega t)\end{bmatrix} \quad (39)$$

$$V_{dq2}=V_{\alpha\beta}\begin{bmatrix}-\cos(\omega t) & -\sin(\omega t)\\ \sin(\omega t) & -\cos(\omega t)\end{bmatrix} \quad (40)$$

It is verified based on equations (39) and (40) that:

$$V_{dq1}=-V_{dq2} \quad (41)$$

$$V_{dq1}=V_1\begin{bmatrix}\cos(\phi_1)\\ \sin\phi_1)\end{bmatrix}+V_2\begin{bmatrix}\cos(\phi_2) & \sin(\phi_2)\\ -\sin(\phi_2) & \cos(\phi_2)\end{bmatrix}\begin{bmatrix}\cos(2\omega t)\\ \sin(2\omega t)\end{bmatrix} \quad (42)$$

$$V_{dq1}=V_1\begin{bmatrix}\cos(\phi_1)\\ \sin\phi_1)\end{bmatrix}+V_{d2}\begin{bmatrix}\cos(2\omega t)\\ -\sin(2\omega t)\end{bmatrix}+V_{q2}\begin{bmatrix}\sin(2\omega t)\\ \cos(2\omega t)\end{bmatrix} \quad (43)$$

$$V_{dq2}=V_2\begin{bmatrix}\cos(\phi_2)\\ \sin\phi_2)\end{bmatrix}-V_{d1}\begin{bmatrix}\cos(2\omega t)\\ \sin(2\omega t)\end{bmatrix}+V_{q1}\begin{bmatrix}\sin(2\omega t)\\ -\cos(2\omega t)\end{bmatrix} \quad (44)$$

Equations (44) and (43), respectively, are used to express the negative and positive sequences. The instantaneous PQ theory equations obtained by substituting decoupled current and voltage values for Park's transformation are as follows:

$$P_1=\frac{3}{2}\begin{bmatrix}V_{d1} & -V_{q1} & V_{d2} & V_{q2}\end{bmatrix}\begin{bmatrix}i_{q2}\\ i_{d2}\\ i_{q1}\\ i_{d1}\end{bmatrix} \quad (45)$$

$$Q_1=P_2=\frac{3}{2}\begin{bmatrix}V_{d1} & V_{q1} & V_{d2} & V_{q2}\end{bmatrix}\begin{bmatrix}i_{d2}\\ i_{q2}\\ i_{d1}\\ i_{q1}\end{bmatrix} \quad (46)$$

$$Q_2=\frac{3}{2}\begin{bmatrix}V_{d1} & -V_{q1} & V_{q2} & -V_{d2}\end{bmatrix}\begin{bmatrix}i_{q2}\\ i_{d2}\\ i_{d1}\\ i_{q1}\end{bmatrix} \quad (47)$$

Decoupled voltage and current are the basis for producing the reference signal, which is provided as:

$$P_0=\frac{3}{2}\begin{bmatrix}V_{d1} & -V_{q1} & -V_{d2} & V_{q2}\end{bmatrix}\begin{bmatrix}i_{q2}\\ i_{d2}\\ i_{q1}\\ i_{d1}\end{bmatrix} \quad (48)$$

$$Q_0=P_2=\frac{3}{2}\begin{bmatrix}V_{d1} & V_{q1} & V_{d2} & V_{q2}\end{bmatrix}\begin{bmatrix}i_{d2}\\ i_{q2}\\ i_{d1}\\ i_{q1}\end{bmatrix} \quad (49)$$

4 Results and Discussions

Since sensitive loads are becoming more and more common in distributed power systems, there has been a lot of focus on the need for better power quality. This paper demonstrates the application of a PV-UPQC with suitable control mechanisms to raise the PQ. An adaptive PI controller stabilizes the increased voltage output from the Re-lift Luo converter, which connects the PV to the UPQC. Moreover, the DDSRF theory and the CT2FLC were utilized to manage UPQC.

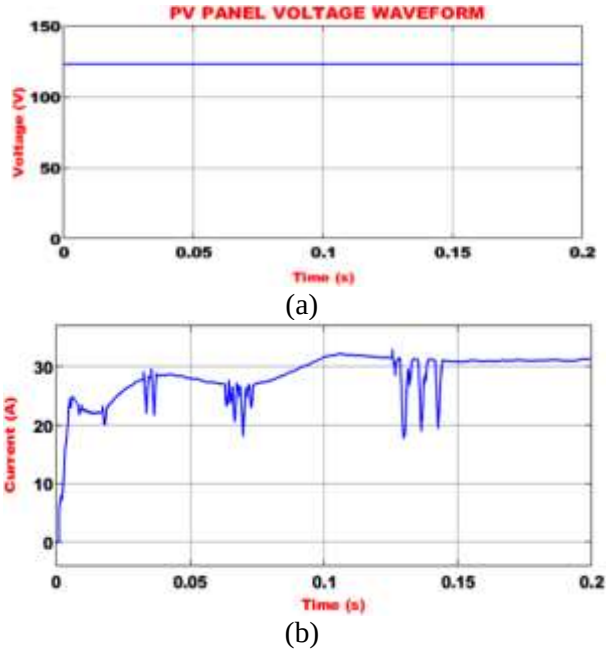

(a)

(b)

Fig 10: Waveforms of (a) PV panel voltage (b) PV panel current

As seen in Figure 10(a), the re-lift Luo converter receives an input of 125 V from the PV panel to produce a higher DC output voltage. Figure 10(b) illustrates how the different operating circumstances cause the PV panel output current to change suddenly before stabilizing at approximately 32 A.

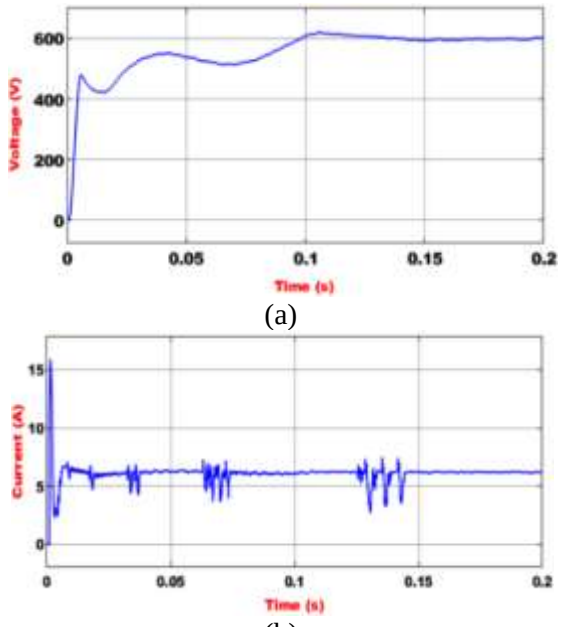

(a)

(b)

Fig 11: Representation of the (a) Converter output voltage and (b) Converter output current

With the help of an adaptive PI controller, the re-lift Luo converter produces a stable output voltage and output current of 600 V and 7 A, respectively, as shown in Figure 11.

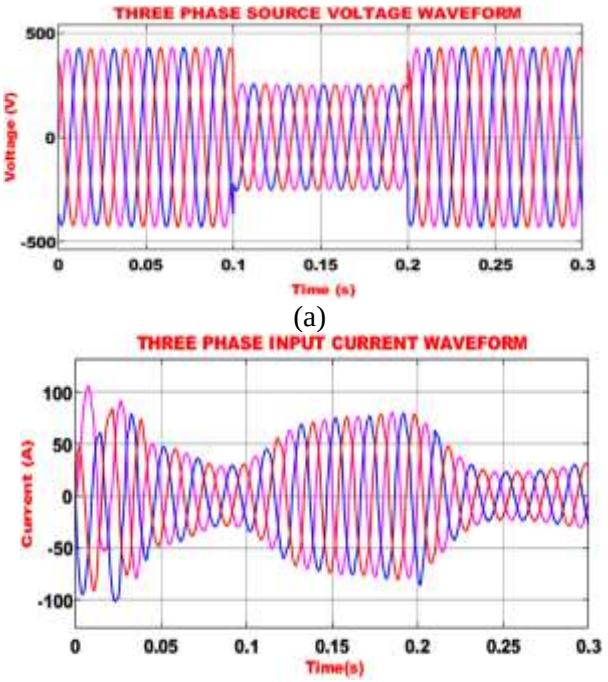

(a)

(b)

Fig 12: Illustration of the (a) Three-phase source voltage and (b) Three phase source current

It is evident from Figure 12(a) that an approximate 400 V AC voltage is maintained continuously for 0.1 seconds, after which it decreases to 250 V as a result of PQ problems. Because of PQ problems, the three-phase source current is highly unstable and distorted, as seen in Figure 12(b).

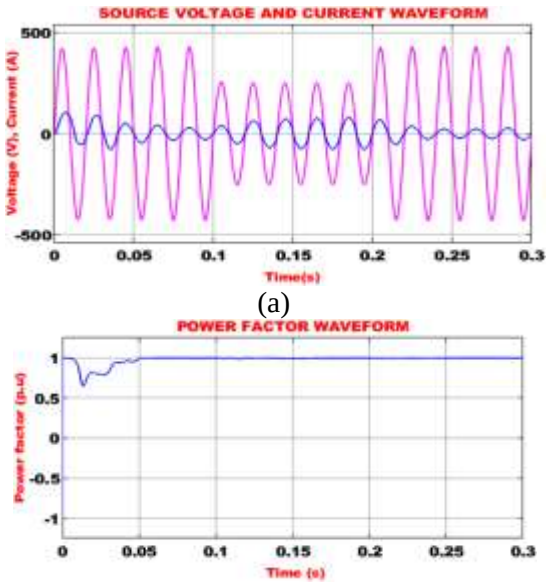

(a)

(b)

Fig 13: Representation of the (a) Source voltage and current (b) Power factor

Figure 13(b) makes it evident that CT2FLC-based UPQC enhances power quality and facilitates the achievement of the unity power factor. Figure 13(a) displays the source voltage and current waveforms.

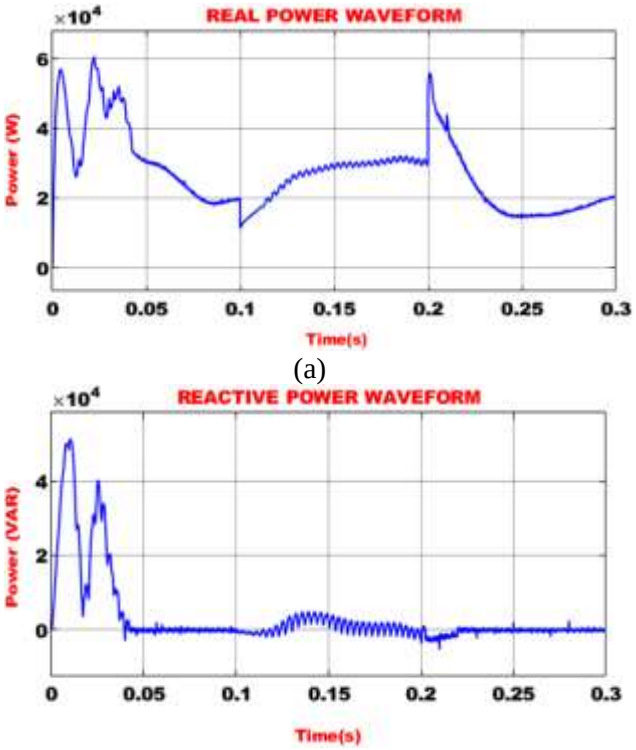

(a)

(b)

Fig. 14: Illustration of the (a) real power and (b) reactive power

Real power and reactive power are depicted in Figure 14(a) and Figure 14(b), respectively. The real and reactive power are distortion-free after applying the recommended control approach, despite the waveform's early power changes.

A steady load voltage of 400 V and a steady load current of around 35 A is continuously maintained distortion-free with the suggested PQ enhancement technique. Thus, as illustrated in Figure 15, the suggested PV-UPQC with CT2FLC design successfully and efficiently raises the PQ on the load side.

A shunt converter, which serves as a controlled current source, is used to ensure effective load current harmonics compensation once the proper quantity of reactive current is injected into the line. As indicated in Figure 16(a), to reduce the current harmonics that are present on the load side, a reference current of 45 A is created between 0.15s and 0.2s.

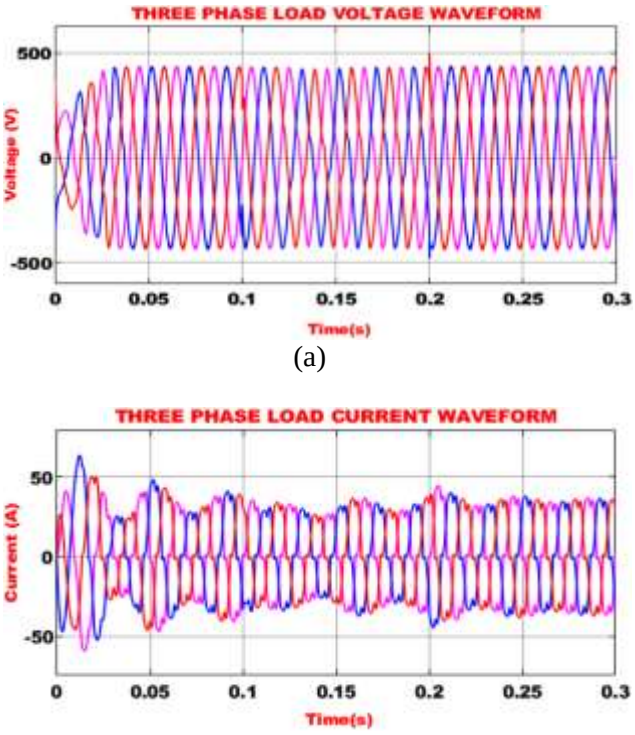

(a)

(b)

Fig. 15: Representation of the (a) load voltage and (b) load current

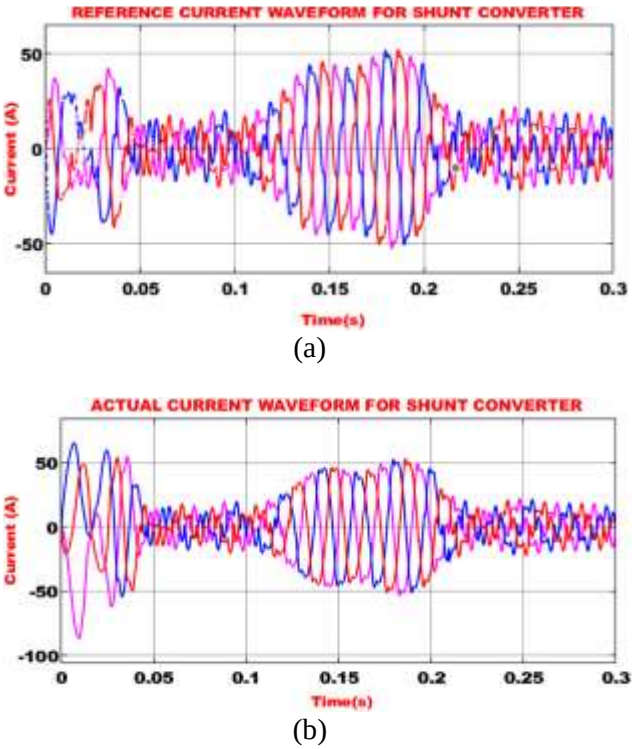

(a)

(b)

Fig. 16: Shunt converter results representation (a) Reference current and (b) actual current

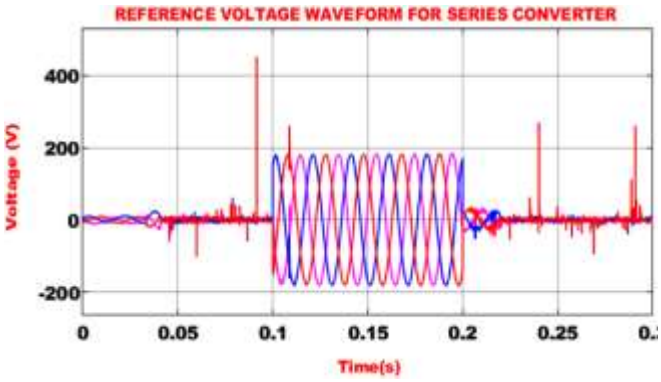

(a)

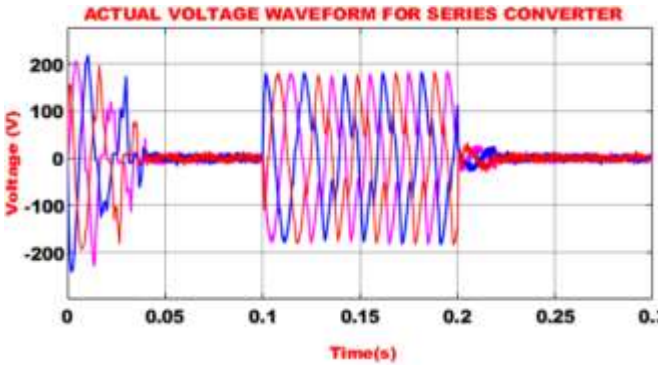

(b)

Fig. 17: Representation of series converter's (a) Reference voltage and (b) actual voltage

Using a series converter, effective voltage sag compensation is accomplished by injecting the desired magnitude of voltage into the line. From 0.1s to 0.2s, a steady voltage of 180 V is obtained without any abnormalities, as seen in Figure 17(b). Figure 18 shows the estimated THD of 3.25%.

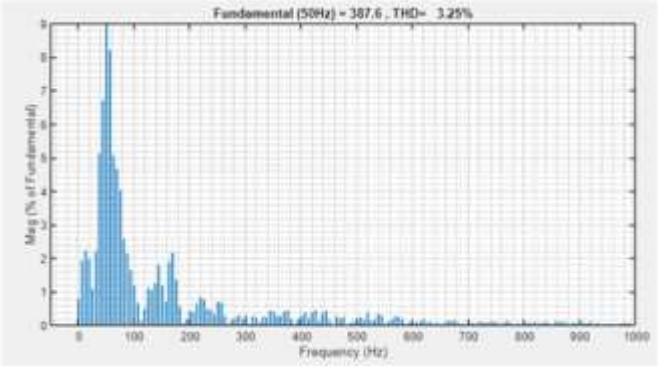

Fig. 18: Representation of the total harmonic distortion

(a)

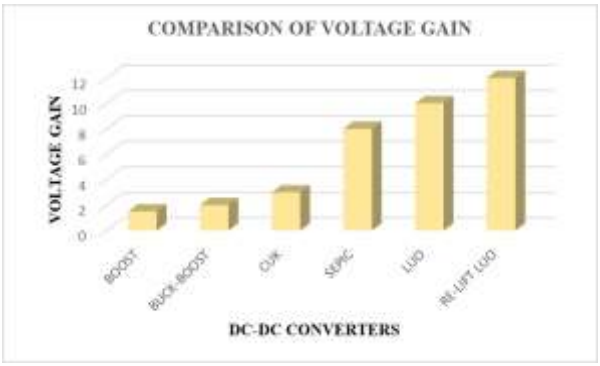

(b)

Fig. 19: Illustrates the dc-to-dc converters (a) Efficiency, and (b) Voltage gain comparisons

Based on voltage gain and efficiency, the Re-lift Luo converter's operational performance is compared to several other current converters, as illustrated in Figure 19. The Re-lift Luo converter operates at an outstanding 95% efficiency and a voltage gain ratio of 1:12.

5 Conclusion

Several PQ problems in power systems have developed as a result of the growing use of sensitive power electronic equipment. If these issues are not successfully fixed, the system as a whole may eventually fail, causing large economic losses. When PV-based power generation and UPQC are integrated, clean energy with higher PQ is produced. Voltage instability is caused by the PV system because it is a discontinuous low power source. The voltage produced by the PV is enhanced and stabilized by the adaptive PI controller and the re-lift Luo converter. Moreover, CT2FLC and DDSRF theory are used to guarantee UPQC control. The output from MATLAB simulations indicates that the planned UPQC setup is effective in improving both the load side and source side PQ concerns. Re-lift Luo converters have remarkable 95% efficiency and a high voltage gain of 1:12.

References:

[1] Montoya, F. G., Baños, R., Alcayde, A., Montoya, M. G., & Manzano-Agugliaro, F. (2018). Power quality: Scientific collaboration networks and research trends. *Energies*, 11(8), 2067.

[2] Xi, Y., Li, Z., Zeng, X., Tang, X., Liu, Q., & Xiao, H. (2018). Detection of power quality disturbances using an adaptive process noise covariance Kalman filter. *Digital Signal Processing*, 76, 34-49.

[3] Devassy, S., & Singh, B. (2017). Design and performance analysis of three-phase solar PV integrated UPQC. *IEEE Transactions on Industry Applications*, 54(1), 73-81.

[4] Katuri, R., & Gorantla, S. (2020). Modeling and analysis of hybrid controller by combining MFB with FLC implemented to ultracapacitor-based electric vehicle. *WSEAS Transactions on Power Systems*, 15, 21-29, https://doi.org/10.37394/232016.2020.15.3.

[5] Kazmierkowski, M. P. (2015). Power quality: Problems and mitigation techniques [book news]. *IEEE Industrial Electronics Magazine*, 9(2), 62-62.

[6] Kumar Agarwal, R., Hussain, I., & Singh, B. (2017). Three-phase single-stage grid tied solar PV ECS using PLL-less fast CTF control technique. *IET Power Electronics*, 10(2), 178-188.

[7] Beniwal, N., Hussain, I., & Singh, B. (2018). Second-order volterra-filter-based control of a solar PV-DSTATCOM system to achieve Lyapunov's stability. *IEEE Transactions on Industry Applications*, 55(1), 670-679.

[8] Modi, G., Kumar, S., & Singh, B. (2019). Improved Widrow–Hoff based adaptive control of multiobjective PV-DSTATCOM system. *IEEE Transactions on Industry Applications*, 56(2), 1930-1939.

[9] Ye, J., & Gooi, H. B. (2019). Phase angle control based three-phase DVR with power factor correction at point of common coupling. *Journal of Modern Power Systems and Clean Energy*, 8(1), 179-186.

[10] Moghassemi, A., Padmanaban, S., Ramachandaramurthy, V. K., Mitolo, M., & Benbouzid, M. (2020). A novel solar photovoltaic fed Trans ZSI-DVR for power quality improvement of grid-connected PV systems. *IEEE Access*, 9, 7263-7279.

[11] Molla, E. M., & Kuo, C. C. (2020). Voltage sag enhancement of grid connected hybrid PV-wind power system using battery and SMES based dynamic voltage restorer. *IEEE Access*, 8, 130003-130013.

[12] Ray, P., Ray, P. K., & Dash, S. K. (2021). Power quality enhancement and power flow analysis of a PV integrated UPQC system in a distribution network. *IEEE Transactions on Industry Applications*, 58(1), 201-211.

[13] Yu, J., Xu, Y., Li, Y., & Liu, Q. (2020). An inductive hybrid UPQC for power quality management in premium-power-supply-required applications. *IEEE Access*, 8, 113342-113354.

[14] Sefa, I., Altin, N. E. C. M. I., Ozdemir, S., & Kaplan, O. R. H. A. N. (2015). Fuzzy PI controlled inverter for grid interactive renewable energy systems. *IET Renewable Power Generation*, 9(7), 729-738.

[15] Bayhan, S., Demirbas, S., & Abu-Rub, H. (2016). Fuzzy-PI-based sensorless frequency and voltage controller for doubly fed induction generator connected to a DC microgrid. *IET Renewable Power Generation*, 10(8), 1069-1077.

[16] Katuri, R., & Gorantla, S. (2023). Design and comparative analysis of controllers implemented to hybrid energy storage system based solar-powered electric vehicle. *IETE Journal of Research*, 69(7), 4566-4588.

[17] Essamudin Ali Ebrahim (2023). Real-Time Implementation of BLDC Motor-Based Intelligent Tracking Control Fed from PV-Array for E-Bike Applications. *WSEAS Transactions on Power Systems*, 18, 270-281, https://doi.org/10.37394/232016.2023.18.28.

[18] Ekaterina Gospodinova (2023). Mathematical Modeling and Planning of Energy Production using a Neural Network. *WSEAS Transactions on Power Systems*, 18, 39-48, https://doi.org/10.37394/232016.2023.18.5.

[19] C. Pica, R. Munteanu, S. Pavel and H. Beleiu (2018), "Modeling of Photovoltaic Panels," *2018 International Conference and Exposition on Electrical and Power Engineering (EPE)*, Iasi, Romania, pp. 0769-0773.

[20] Antonino Fotia, Raffaele Pucinotti, Vincenzo Barrile (2022). Detection of Steel Structures Degradation through a UAVs and Artificial Intelligence Automated System. *WSEAS Transactions on Circuits and Systems*, 21, 231-237, https://doi.org/10.37394/23201.2022.21.25.

[21] Atanas N. Kostadinov, Guennadi A. Kouzaev (2022). A Novel Processor for Artificial Intelligence Acceleration. *WSEAS Transactions on Circuits and Systems*, 21,

125-141, https://doi.org/10.37394/23201.2022.21.14.

[22] Y. Li and A. Q. Huang, "Huang-Pair (2021). A New High Voltage Diode Concept and Its Demonstration," in *IEEE Transactions on Power Electronics*, vol. 36, no. 8, pp. 8653-8657.

[23] Y. He and D. J. Perreault (2020), "Diode Evaluation and Series Diode Balancing for High-Voltage High-Frequency Power Converters," in *IEEE Transactions on Power Electronics*, vol. 35, no. 6, pp. 6301-6314.

Contribution of Individual Authors to the Creation of a Scientific Article (Ghostwriting Policy)

The authors equally contributed to the present research, at all stages from the formulation of the problem to the final findings and solution.

Sources of Funding for Research Presented in a Scientific Article or Scientific Article Itself

No funding was received for conducting this study.

Conflict of Interest

The authors have no conflicts of interest to declare.